Impacts of Sea Ice Leads on Sea Salt Aerosols and Atmospheric Chemistry in the Arctic

Erin J. Emme[1,*]; Hannah M. Horowitz[1,2,*]

[1]**Department of Civil and Environmental Engineering, University of Illinois Urbana-Champaign, Urbana, Illinois, USA**

[2]**Department of Atmospheric Science, University of Illinois Urbana-Champaign, Urbana, Illinois, USA**

For submission to

Atmospheric Chemistry and Physics

October 9, 2024

*Corresponding authors: Erin J. Emme, emme2@illinois.edu, and Hannah M. Horowitz, hmhorow@illinois.edu.

Impacts of Sea Ice Leads on Sea Salt Aerosols and Atmospheric Chemistry in the Arctic

Erin J. Emme[1], Hannah M. Horowitz[1,2]

[1]Department of Civil and Environmental Engineering, University of Illinois at Urbana-Champaign, Urbana, 61801, USA

[2]Department of Atmospheric Sciences, University of Illinois at Urbana-Champaign, Urbana, 61801, USA

Correspondence to: **Erin J. Emme (emme@illinois.edu) and Hannah Horowitz (hmhorow@illinois.edu)**

Abstract. The processes contributing to Arctic cold season (November-April) sea salt aerosols (SSA) remain uncertain. Observations from coastal Alaska suggest emissions from open leads in sea ice, which are not included in climate models, may play a dominant role. Their Arctic-wide significance has not yet been quantified. Here, we create an emissions parameterization of SSA from leads by combining satellite data of lead area (the AMSR-E product) and a chemical transport model (GEOS-Chem) to quantify pan-Arctic SSA emissions from leads during the cold season from 2002-2008 and predict their impacts on atmospheric chemistry, evaluating the results of our simulated SSA against in-situ observations. The AMSR-E product detects large leads with certainty (>3 km in size) and hence our study is limited to quantifying emissions from large leads. Lead emissions vary seasonally and interannually. Simulated total monthly SSA emissions increase by 1.1-1.8% (≥60°N latitude) and 5.6-7.5% (≥75°N) for the 2002-2008 cold season. SSA concentrations increase primarily at the location of leads, where standard model concentrations are low. GEOS-Chem overestimates SSA concentrations at Arctic sites compared to ground observations even when lead emissions are not included, suggesting underestimation of SSA sinks and/or uncertainties in SSA emissions from blowing snow and open ocean. Multi-year monthly mean surface bromine atom (Br) concentrations increase 2.8-8.8% due to SSAs from leads for the 2002-2008 cold season. Changes in ozone concentrations are negligible. While leads contribute <10% to Arctic-wide SSA emissions in the years 2002-2008, these emissions occur in regions of low background aerosol concentrations. Leads may increase in frequency under future climate change, which could increase SSA emissions from leads.

Short Summary

There is uncertainty in the sources of Arctic cold season (November-April) sea salt aerosols. Using a chemical transport model and satellite observations, we quantify Arctic-wide sea salt aerosol emissions from fractures in sea ice, called open sea ice leads, and their atmospheric

chemistry impacts for the cold season. We show sea ice leads contribute to Arctic sea salt aerosols and bromine, especially in under-observed regions.

1. Introduction

Sea salt aerosols (SSA) affect Arctic climate by scattering incoming solar radiation and acting as cloud condensation nuclei and ice nuclei (DeMott et al., 2016; Pierce and Adams, 2006; Quinn et al., 1998). In the Arctic, these processes are relevant during the fall and spring, but negligible during polar night, when there is no sunlight. Long-term measurements have shown that peak SSA concentrations in the Arctic occur during the cold season (Leaitch et al., 2018; Quinn et al., 2002; Schmale et al., 2021). However, the sources and mechanisms of cold season SSA emissions are uncertain, which hinders atmospheric chemistry and climate models from accurately representing polar regions. Recent observations from Utqiaġvik, Alaska have suggested that open leads, or open sea ice fractures, are an important source of cold season SSA emissions (Kirpes et al., 2019; May et al., 2016). Climate change has impacted the Arctic by rapidly decreasing sea ice age and thickness (Intergovernmental Panel On Climate Change, 2023; Sumata et al., 2023; Vaughan et al., 2013), and future projections indicate this will continue (Intergovernmental Panel On Climate Change, 2023), suggesting the amount of open leads will increase in the future due to thinner ice that is prone to fracture. More work is needed to discern the Arctic-wide importance and impacts of SSA emissions from sea ice leads ("lead emissions") on atmospheric chemistry and climate. By combining satellite observations and chemical transport modeling, we quantify the significance and impacts of lead emissions on atmospheric concentrations of SSA and bromine and evaluate simulated SSA against in-situ observations.

While global models have not yet included SSA emissions from leads, several observational studies largely based in Utqiaġvik, Alaska suggest emissions of SSA from leads may be important. Key early observations in the 1970s in Utqiaġvik, by Scott & Levin (1972) and Radke et al. (1976) demonstrated an increase in sodium-containing particles in the presence of open water leads. Since then, more recent measurement studies have quantified SSA emissions from leads. Nilsson et al. (2001) estimate that leads contribute an order of magnitude less than the open ocean to the Arctic SSA flux during the summer months. A multi-year study of observed SSA at Utqiaġvik (May et al., 2016), conducted over all seasons, found that leads are a significant contributor to SSA through wind-driven production, increasing the supermicron range in particular, but to a lesser extent than wind-driven production from the open ocean. Willis et al. (2018) suggest

87 that lead emissions are more important in winter and early spring as winds over the Northern
88 oceans are at their highest. Kirpes et al. (2019) also convey the importance of seasonality,
89 identifying SSA produced by local leads as the dominant aerosol source in the coastal Alaskan
90 Arctic during winter months. Chen et al. (2022), focusing on the spring, shows at Utqiaġvik that
91 leads were present locally throughout the study and contributed to sea spray aerosol production.
92 As ground-based observations in the Arctic are mainly limited to coastal stations, such as
93 Utqiaġvik, it is difficult to estimate the significance and impacts of lead emissions over the entire
94 Arctic. Representing Arctic-wide emissions from leads in a global chemical transport model,
95 especially during the cold season, will help discern whether lead emissions and their impacts on
96 atmospheric chemistry are significant enough to warrant inclusion in chemistry as well as climate
97 models.

98

99 Other modeling studies in the Arctic and observations primarily from Antarctica suggest blowing
100 snow is a potential major contributor of cold season SSA in polar regions. Blowing snow SSA
101 comes from saline snow over sea ice that is swept up by wind; the snow becomes salty through
102 the upward movement of brine from sea ice to the snow surface, incorporation of frost flowers,
103 and deposition of SSA from the nearby open ocean (Domine et al., 2004). In two chemical
104 transport models, the inclusion of additional SSA emissions from blowing snow brought simulated
105 SSA mass concentrations closer to what was observed (Confer et al., 2023; Huang et al., 2018;
106 Huang and Jaeglé, 2017; Rhodes et al., 2017). Other potential sources of cold season SSA, such
107 as frost flowers, have been found to be insignificant (Alvarez-Aviles et al., 2008; Roscoe et al.,
108 2011; Yang et al., 2017). Incorporating blowing snow SSA emissions into models has shown how
109 missing sources of SSA in the Arctic can have a significant impact on atmospheric chemistry; for
110 example, Huang et al. (2020) show bromine released by blowing snow impacts modeled
111 springtime bromine activation and ozone depletion events. The strong observational evidence
112 that leads contribute to cold season SSA and the impact of blowing snow SSA on modeled Arctic
113 atmospheric chemistry suggests there is a need to assess the potential impacts of lead emissions,
114 which are currently missing from global chemistry and climate models. One study incorporated
115 SSA emissions from leads in a chemical transport model (WRF-Chem), but the study was limited
116 to the 400 km^2 area surrounding Utqiaġvik, Alaska and used ERA-5 reanalysis sea ice fraction to
117 define the presence of leads (Ioannidis et al., 2023) They find open leads are the primary source
118 of fresh and aged SSA in Utqiaġvik, Alaska during the cold season, consistent with the
119 observational analyses by May et al. (2016) and Kirpes et al. (2019).

120

121 SSA play a critical role in Arctic tropospheric chemistry. SSA debromination is the main global
122 source of reactive bromine in the troposphere (Wang et al., 2021). Reactive bromine chemistry
123 has been attributed to the rapid depletion of ozone in the Arctic springtime, which reaches a
124 maximum in March-April (Simpson et al., 2007). In particular, bromine atom (Br) is key to these
125 ozone depletion events; it is produced through the photolysis of Br_2, which is sourced from SSA
126 debromination and snowpack chemistry (Abbatt et al., 2012; Dibb et al., 2010; Pratt et al., 2013;
127 Stutz et al., 2011). Swanson et al. (2022) show improved springtime model-observation
128 agreement of BrO by including a snowpack photochemistry mechanism based on multiple field
129 observations in a global chemical transport model. While on a global scale, reaction of OH with
130 other SSA-sourced bromine species can also produce Br (Wang et al., 2021), this is minor in polar
131 regions due to low OH concentrations. Br rapidly depletes ozone through heterogeneous
132 reactions, which produces BrO that can photolyze to reform Br, creating a catalytic ozone-
133 depletion cycle (Simpson et al., 2007).

134

135 Here, we estimate the pan-Arctic contribution of leads to total SSA emissions during the cold
136 season for the years 2002-2008, by using satellite observations of lead area to parameterize lead-
137 based SSA production in the global chemical transport model GEOS-Chem. We evaluate
138 simulated SSA concentrations against observations and predict the impacts of lead SSA
139 emissions on atmospheric chemistry, including concentrations of Br and ozone.

140

141 **2. Methods**

142

143 *2.1 Satellite Data of Lead Area Fractions*

144

145 In this study, we use satellite data of lead area fractions to inform the GEOS-Chem chemical
146 transport model (next section) of where leads are present. The Advanced Microwave Scanning
147 Radiometer-Earth Observation System (AMSR-E) sensor aboard NASA's Aqua satellite recorded
148 brightness temperatures from Earth from 2002-2011 at six different frequencies
149 (https://www.cen.uni-hamburg.de/en/icdc/data/cryosphere/lead-area-fraction-amsre.html)
150 (Integrated Climate Data Center (ICDC) et al., n.d.), which are converted to lead area fractions
151 following the algorithm of Röhrs and Kaleschke (2012). This method of detection can only be
152 applied to the Arctic freezing season (November-April) due to surface melt of the sea ice modifying
153 the sea ice emissivity from May-October, which affects the lead detection algorithm. Daily data is
154 available at 6.25 km horizontal resolution, as the algorithm is not limited by cloud cover. The

155 AMSR-E satellite data is regridded to 0.5°x0.625° from 6.25x6.25 km using a distance-weighted
156 average remapping for consistency with the emission model's resolution (see Sect. 2.2 below for
157 model details). For the rare individual days with missing data in the dataset (0.8%), we use the
158 average lead area fraction for that month. The lead area fraction includes open water leads and
159 thin ice-covered leads 3 km and wider. The data spans latitudes 41° to 90°N, though a majority
160 of Arctic sea ice lies above 60°N and leads are therefore unlikely to be present at lower latitudes.
161
162 We use the AMSR-E lead area product for this study as it avoids cloud interference when
163 detecting leads and provides nearly consistent daily resolution. A limited quantitative validation
164 by Röhrs and Kaleschke (2012) of one day (March 21, 2006) of the AMSR-E product against
165 Moderate Resolution Image Spectroradiometer (MODIS) showed 50% of the total lead area
166 visible in 500 m MODIS images was detected in the AMSR-E product. Leads greater than 3 km
167 in size ("large leads") were detected with certainty for the AMSR-E product (Röhrs and Kaleschke,
168 2012), so our results effectively estimate emissions from large leads only.
169
170 *2.2 GEOS-Chem: global chemical transport model*
171
172 Here we use the 3-D atmospheric transport model GEOS-Chem (geos-chem.org) version 13.2.1
173 (https://doi.org/10.5281/zenodo.5500717)   Within GEOS-Chem, the Harmonized Emissions
174 Component (HEMCO) computes emissions for different sources, regions, and species (Keller et
175 al., 2014). GEOS-Chem and HEMCO are driven by Modern-Era Retrospective Analysis for
176 Research and Applications (MERRA-2) (Gelaro et al., 2017) meteorological fields from the NASA
177 Global Modeling and Assimilation Office (GMAO), which is reanalysis meteorological data
178 assimilated from various observational sources (i.e., satellite, aircraft campaigns, and ground
179 stations) providing variables such as temperature, wind, precipitation, and humidity. GEOS-Chem
180 represents one-way interactions between the MERRA-2 meteorology and chemical constituents,
181 meaning the meteorological conditions can affect the concentration of chemical species but not
182 vice versa.
183
184 SSA emissions calculations for the open ocean use a wind- (Gong, 2003; Monahan et al., 1986)-
185 and sea-surface-temperature-dependent (Jaeglé et al., 2011) source function. In polar regions,
186 SSA emissions from blowing snow are also included (Huang and Jaeglé, 2017). SSA have two
187 size bins: coarse mode (SALC; r= 0.5 to 10 µm) and accumulation mode (SALA; r= 0.1 to 0.5
188 µm). For gas and aerosol species, wet deposition (both rain and snow) includes washout and

189   rainout in convective and large-scale stratiform precipitation (Amos et al., 2012; Liu et al., 2001;

190   Wang et al., 2014). From November to April in the Arctic, wet deposition is mainly in the form of

191   snow (Screen and Simmonds, 2012). Dry deposition of gas and aerosol species follows a

192   resistance-in-series approach, and includes gravitational settling of sea salt (Jaeglé et al., 2011;

193   Pound et al., 2020; Wang et al., 1998; Zhang et al., 2001). Coupled gas- and multiphase-reactive

194   halogen chemistry, including sea salt debromination, acid displacement, and photolysis and

195   oxidation of gas-phase inorganic bromine and chlorine species, is described in Wang et al. (2021).

196   This version of GEOS-Chem does not include snowpack chemistry as a source of reactive

197   bromine in the standard model.

198

199   We parameterize SSA emissions from leads with the same function as the open ocean emissions

200   from Jaeglé et al. (2011) (Eq. (S.1) in the Supplemental Information (SI)), scaled by the fractional

201   area of leads in each grid cell from the AMSR-E satellite data. The Jaeglé et al. (2011) function is

202   empirically derived to best match global observations in GEOS-Chem. We assume that leads emit

203   SSA at an equal rate as a function of lead area. This lead emissions parameterization is a unique

204   wind- and SST-dependent source function for calculating lead emissions, driven by satellite

205   observations defining the presence of leads. Figure 1 shows an example of the daily temporal

206   frequency and spatial resolution of the AMSR-E satellite data (both the raw (a) and regridded (b))

207   used to drive the model.

208

209

AMSR-E Lead Area Fraction
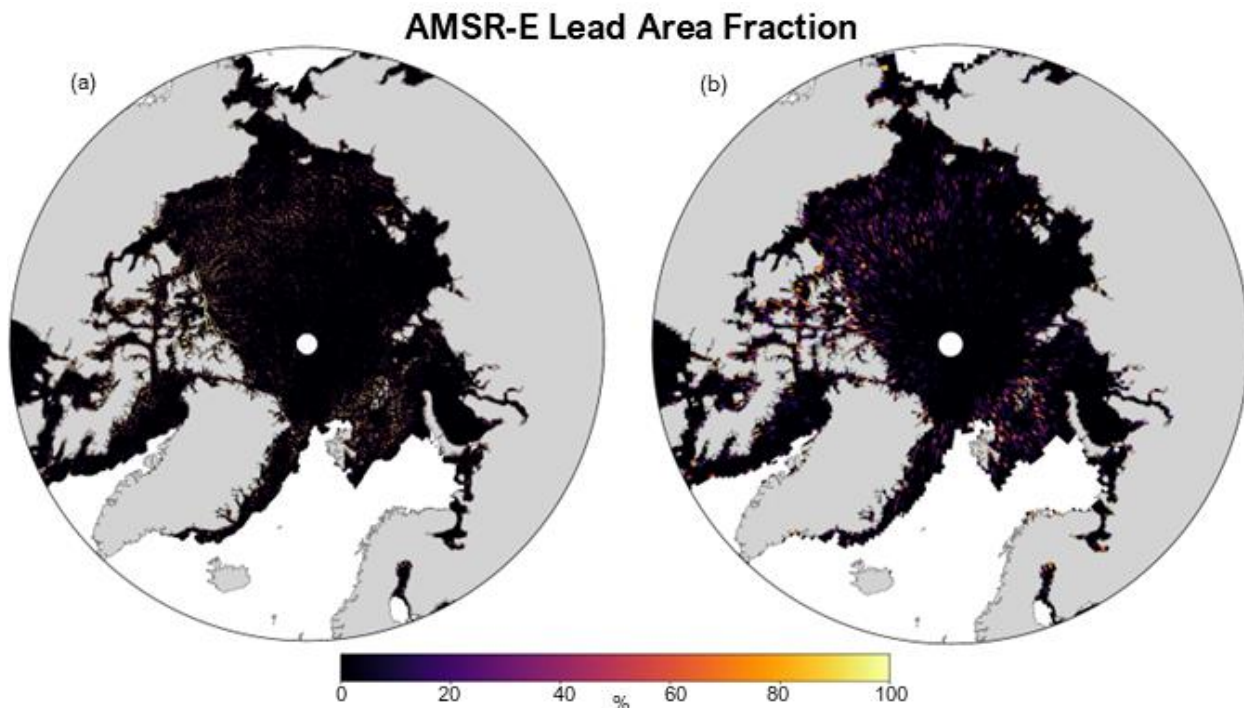
210

211   **Figure 1-** Map of AMSR-E daily lead area fraction in percent (%) for November 1, 2002, both raw

212   (6.25-km resolution) (a) and re-gridded (0.5˚x0.625˚ resolution) (b).

213

214   We first calculate SSA emissions at the highest resolution of HEMCO (0.5°x0.625°), which is the

215   native resolution of MERRA-2. Two sets of emissions are calculated: (1) the standard emissions

216   only (i.e., open ocean and blowing snow SSA emissions, the "standard" case); (2) SSA emissions

217   with lead emissions added ("standard + leads" case). Each set of emissions are then implemented

218   separately into GEOS-Chem "offline" to ensure total SSA emissions are properly scaled and

219   distributed and not influenced by the resolution-dependence of the wind speed (Lin et al., 2021).

220   GEOS-Chem is run at the highest global horizontal (2° latitude x 2.5° longitude) and vertical (72

221   vertical levels) resolution. The absolute difference between the standard + leads and standard

222   simulations is the change in SSA emissions or concentration from leads, and we present the

223   percent change due to leads (%) as calculated with Eq. (1).

224

225    $Percent\ change\ due\ to\ leads\ (\%) = 100 \times \dfrac{(Standard+leads)_{simulation} - (Standard)_{simulation}}{(Standard)_{simulation}}$ (1)

226

227   Simulations are performed for the years 2002-2008, when there is overlap between the AMSR-E

228   satellite data and available observed Arctic SSA concentrations at multiple sites, following one

229   year of initialization. Because satellite observations of lead area fractions begin November 1,

230   2002, we initialize the standard + leads case for GEOS-Chem with standard + leads SSA
231   emissions for one year (November 1, 2002 to November 1, 2003) and then start the simulation
232   for analysis on November 1, 2002, with the spun-up November 1, 2003, initial conditions. For the
233   standard case, the initialization year begins November 1, 2001. For both cases, we simulate SSA
234   concentrations, evaluate against observed concentrations, and assess the impacts of additional
235   lead emissions on atmospheric chemistry. This includes analysis of the change in atmospheric
236   concentrations of bromine atom (Br) and ozone (O_3). For model evaluation, GEOS-Chem does
237   not track sodium (Na^+) content for SSA, so we convert simulated SSA to Na^+ mass concentrations
238   using a factor of $\frac{1}{3.256}$, which is based on the mass ratio of Na^+ in seawater (Confer et al., 2023;
239   Huang and Jaeglé, 2017; Riley and Chester, 1971).

240

241   *2.3 In-Situ Observations of Arctic Sea Salt Aerosol Concentrations*

242

243   We evaluate simulated concentrations of SSA from GEOS-Chem, converted to Na^+
244   concentrations, against in situ observations of Na^+ concentrations at 4 Arctic sampling sites:
245   Utqiaġvik, Alaska (71.3°N, 156.6°W; 11m a.s.l.) (Quinn et al., 2002); Zeppelin Mountain, Svalbard,
246   Norway (78.9°N, 11.9°E; 475m a.s.l.) (World Meteorological Organization (WMO), 2003); Alert,
247   Nunavut, Canada (82.5°N, 62.5°W; 210m a.s.l.) (World Meteorological Organization (WMO),
248   2003); Pallas (Matorova), Helsinki, Finland (68 °N, 24.24 °E; 340m a.s.l.) (Salmi, 2018). These
249   observations are available for the time period of this study (November-April from 2002-2008,
250   except for Pallas station, 2003-2008). In winter months, the Utqiaġvik, Zeppelin, and Alert coastal
251   sites border mostly ice-covered ocean (Huang and Jaeglé, 2017). At Utqiaġvik, mass
252   concentrations of Na^+ for submicron and supermicron aerosols are separated, while the other two
253   sites measure the total mass concentration without size distinction. The Na^+ mass concentrations
254   are determined from ion chromatography with uncertainties of 5-11%, or an absolute uncertainty
255   of 0.01 μg/m³ (Quinn et al., 2000; World Meteorological Organization (WMO), 2003). The aerosol
256   sampling frequency is daily at Zeppelin, Utqiaġvik (submicron), and Pallas and weekly at Alert
257   and Utqiaġvik (supermicron).

258

259   3. **Results**

260

261   *3.1 Emissions of Sea Salt Aerosols from Leads*

262
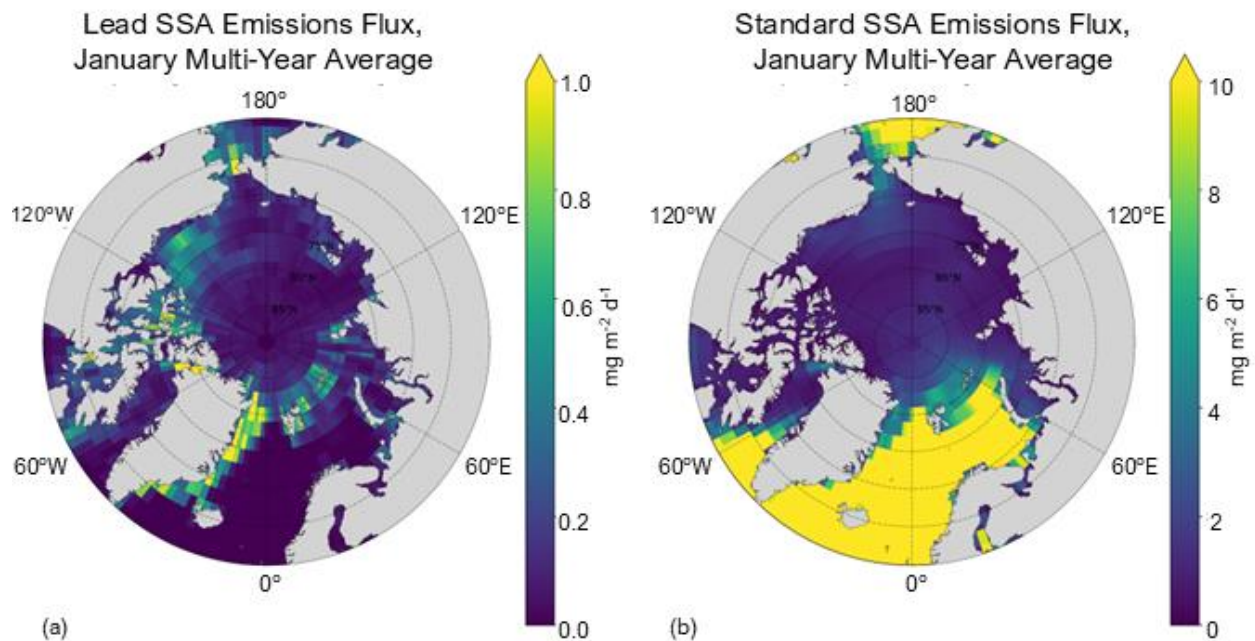
Figure 2- Total (coarse + accumulation mode) lead SSA emissions (a) and standard SSA emissions (b), averaged over 2002-2008 for January. Note the difference in magnitude of the colorbar of (a) and (b).

Figure 2a shows the spatial distribution of multi-year (2002-2008) average lead emissions for the month of January, which is a climatology based on model simulations that use daily resolution lead data (e.g., Fig. 1). We focus Figs. 2 and 4 on the month of January as an example. January is tied for highest lead emissions for latitudes 60°N and greater and second highest for latitudes 75°N and greater (Table 1), and also has the second largest multi-year average lead area (see Fig. S.3b in SI) . Alongside Fig. 2a is the standard model, which includes open ocean and blowing snow emissions (Fig. 2b; see Sect. 2.2). Total emissions are resolution independent and are shown in Fig. 2 for the 2.0°x2.5° resolution of the online atmospheric chemistry simulation. We find the lead emissions and lead area are spatially consistent (Figs. 1 and 2a) and occur in regions where the standard SSA emissions are low (e.g., in the Greenland Sea and parts of the Barents Sea). The percent change in SSA emissions due to leads (calculated with Eq. (1)) is detailed in Table 1; Figs. 4, 5, and S.4 show the percent change in SSA concentration due to leads. Generally, emissions tend to be higher from 70° to 80° N and more concentrated within the Bering Strait, Nares Strait, Wynniatt Bay in the Canadian archipelago, and the eastern Greenland Sea, as opposed to off the coast of Northern Russia and Europe. Month to month, regions where emissions are higher remains similar while the magnitude varies (see Fig. S.1 in SI).

284

Month	Multi-Year (2002-2008) Average Standard Emissions [Gg]		Multi-Year (2002-2008) Average Lead Emissions [Gg] (and corresponding Monthly Percent Change in SSA Emissions due to Leads)	
	≥60°N	≥75°N	≥60°N	≥75°N
November	7800 ± 1000	610 ± 210	82 ± 0.14 (1.1% ± 0.14%)	42 ± 0.13 (6.9% ± 0.13%)
December	8700 ± 1400	640 ± 140	110 ± 0.20 (1.2% ± 0.20%)	48 ±0.32 (7.5% ± 0.32%)
January	8400 ± 1100	670 ± 290	110 ± 0.10 (1.3% ± 0.10%)	46 ± 0.15 (6.9% ± 0.15%)
February	6700 ± 850	510 ± 90	100 ± 0.11 (1.5% ± 0.11%)	37 ± 0.17 (7.2% ± 0.17%)
March	6000 ± 1000	470 ± 66	98 ± 0.074 (1.6% ± 0.07%)	34 ± 0.26 (7.2% ± 0.26%)
April	4200 ± 330	400 ± 61	74 ± 0.081 (1.8% ± 0.08%)	23 ± 0.17 (5.6% ± 0.17%)

285 **Table 1-** Multi-year (2002-2008**)** monthly average standard emissions and lead emissions ±1
286 standard deviation [Gg] and percent change in SSA emissions due to leads ±1 standard deviation
287 in parentheses (calculated using Eq. (1)), averaged for ≥60°N and ≥75°N.

288

289 Table 1 shows the standard and lead emissions in Gg as well as the percent change in multi-year
290 monthly average SSA emissions due to leads for 60° to 90°N latitude (≥60°N) and 75° to 90°N
291 (≥75°N**)**. The standard deviations in Table 1 represent the year-to-year variability in emissions, as
292 the calculation is performed across the 7-year simulation time period for each month. Leads are
293 relatively more important to total SSA emissions at higher latitudes due to large open ocean
294 emissions in the North Atlantic at lower latitudes (Table 1; Fig. 2b) and the spatial variability of the
295 lead emissions (Fig. 2a). The month with the highest contribution to SSA emissions from leads
296 varies with the region being analyzed. The smaller magnitude of standard emissions later in the
297 cold season poleward of 60˚ N make lead emissions relatively more important, with the largest

298   percent increase ≥60° N in SSA emissions due to leads occurring in April. Poleward of 75° N, the

299   lead emissions represent a larger fraction of the standard emissions, resulting in higher percent

300   increases due to leads (~4-6% higher than for ≥60° N). Absolute lead emissions peak in December

301   for ≥75° N latitude, which is also the month with the highest percent increase due to leads ≥75°

302   N, and decrease more than twofold by April. Controlling factors of the lead emissions are

303   discussed in the next paragraph.

304
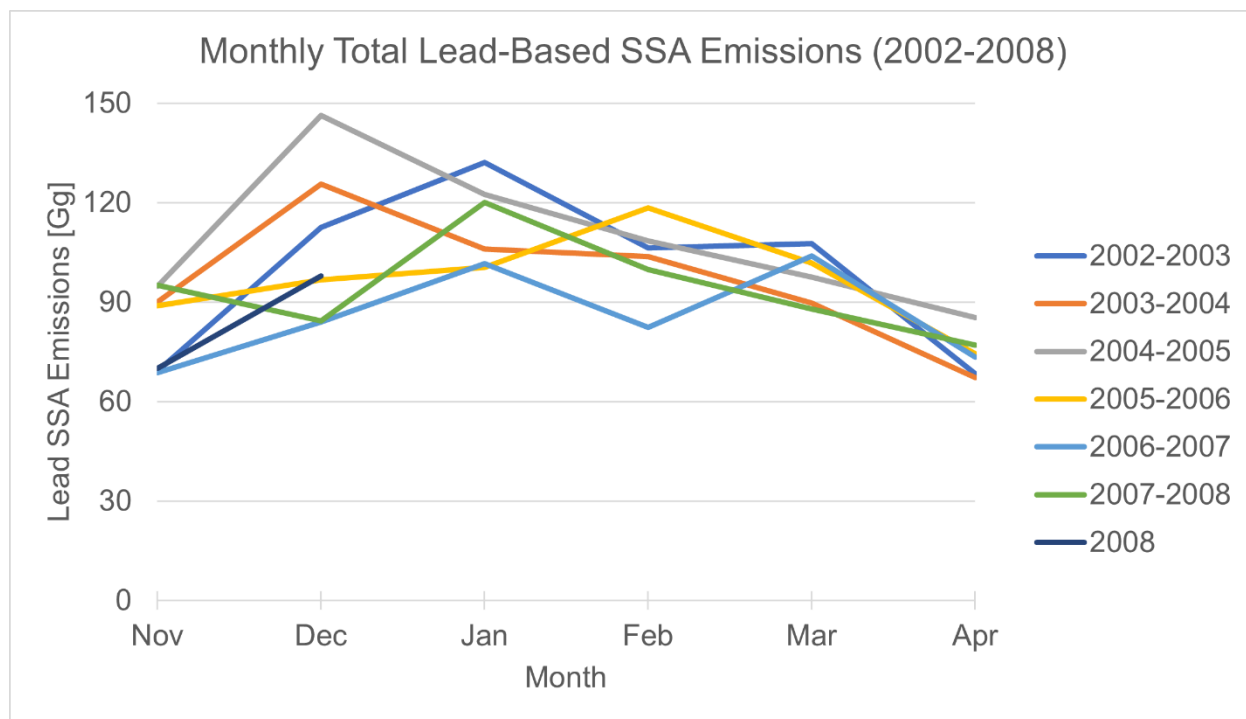
305

306   **Figure 3-** Monthly variations of total (coarse + accumulation mode) lead emissions of SSA during

307   the cold season for 2002-2008. Each line includes November and December of the first year and

308   January through April of the following year, except for the year 2008, which only includes

309   November and December of 2008.

310

311   We find that the magnitude of lead emissions varies by month and year, as well as seasonally

312   (see Fig. 3 and Figs. S.1 and S.2). Monthly total lead emissions and lead area have low correlation

313   (R^2= 0.13, see Fig. S.3), indicating the variance in monthly total lead emissions is dominated by

314   the nonlinear dependencies on wind speed and sea surface temperature (Eq. S.1 in SI), as the

315   lead emissions are calculated with the Jaegle et al. (2011) wind speed and sea surface

316   temperature source function. In most years, lead emissions decrease from January-April, but

317   there is no single month when lead emissions peak each year (Fig. 3). There is also no clear

318   interannual trend in cold season total lead emissions (see Fig. S.2). Lead emissions are lowest in

319   the 2006-2007 cold season and highest in the 2004-2005 cold season (Fig. S.2). In the future,

320   climate models predict that Arctic sea ice will continue to thin (high confidence) and the presence

321   of first-year vs. multi-year sea ice will increase (very high confidence) (Intergovernmental Panel

322   On Climate Change, 2023), suggesting a possible future increasing trend in lead area and

323   therefore lead emissions.

324

325   *3.2 Atmospheric Chemistry Impacts of Sea Ice Leads*

326

327
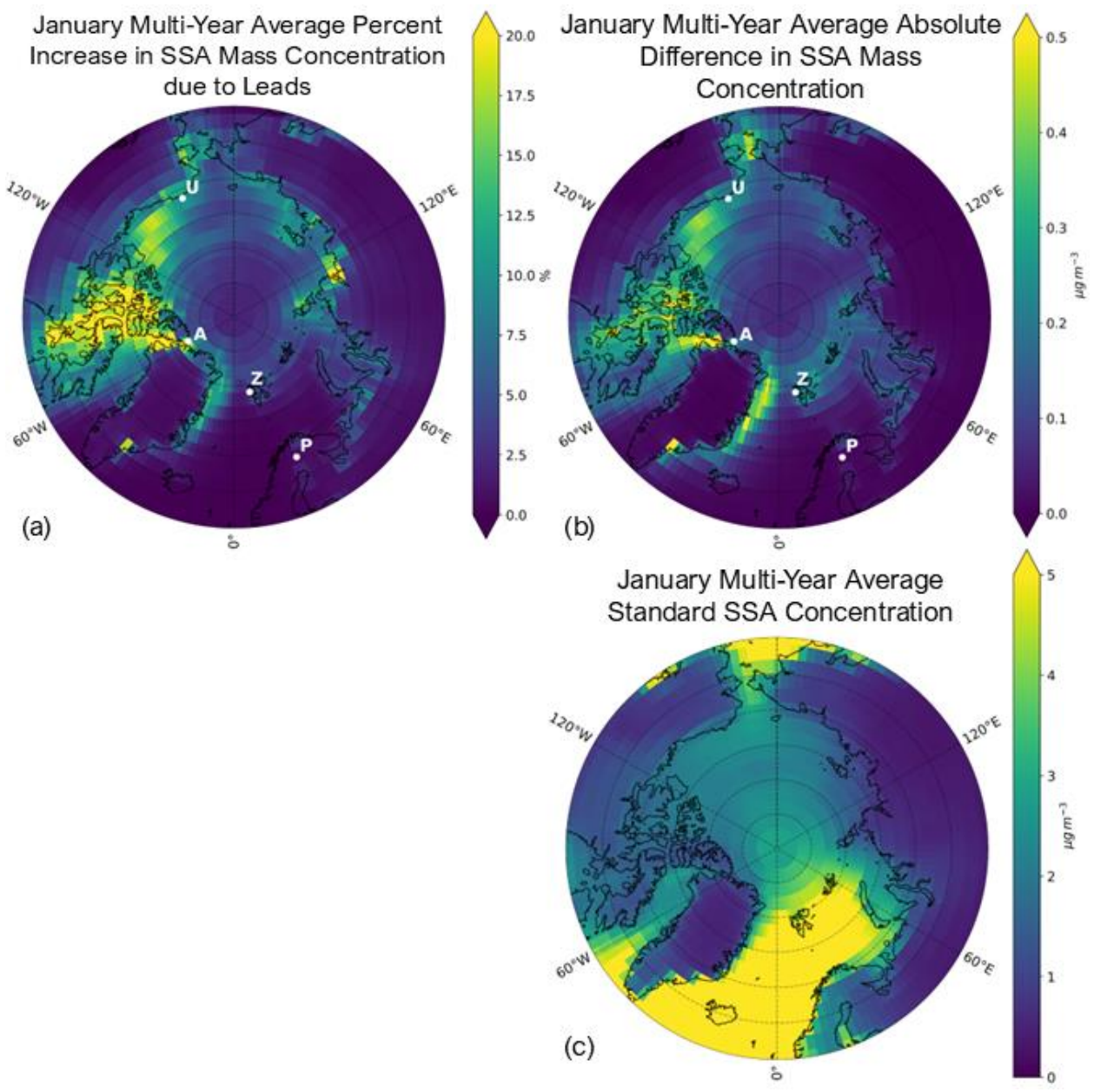
Figure 4- Percent change due to leads (calculated with Eq. (1)) in SSA mass concentration (a), absolute difference between the standard+leads and standard SSA mass concentrations in µg m^{-3} (b), and the standard surface SSA mass concentration in µg m^{-3} (c) for the January multi-year (2002-2008) average. White points in (a) and (b) represent the respective locations of each observational site: Alert, Nunavut, Canada (A); Utqiaġvik, Alaska (U); Zeppelin Mountain, Svalbard, Norway (Z); Pallas (Matorova), Helsinki, Finland (P). Note the difference in magnitude of colorbars (b) and (c).

Figure 4 shows the spatial distribution of the multi-year (2002-2008) average percent change due to leads in surface SSA mass concentration (4a) and the absolute difference in SSA mass concentration between the standard + leads and standard simulations (4b), as well as the standard simulated SSA mass concentration (4c) for the month of January. With the addition of leads, the average Arctic-wide (≥60°N) percent increase in multi-year mean January SSA mass concentrations is 3.3%, and the maximum percent increase in an individual model gridbox is 60.5%. We find that the greatest percent increases due to leads in SSA mass concentrations occur at the location of lead emissions (see Fig. 2a), where the standard concentrations are also very low, except off the eastern coast of Greenland, where the percent increase is reduced due to the high background SSA concentrations in the Greenland Sea (Fig. 4c) from open ocean emissions (Fig. 2b).

Figure 5a shows the average Arctic-wide percent increase and 5c shows the absolute difference due to leads in multi-year monthly mean SSA mass concentration for each cold season month. Averaged poleward of 60°N, the percent increase and absolute difference due to leads in SSA mass concentration remains relatively constant throughout the cold season (Fig. 5a and c). Changes in monthly mean SSA mass concentrations are also higher poleward of 75°N. However, the percent increase in SSA mass concentration for both latitudinal ranges have large spatial variability, as seen in the standard deviation in Fig. 5a. The spatial distribution of the percent increase and absolute difference in SSA mass concentration due to leads remains similar month to month (see Fig. S.4 and S.5 in SI).

359
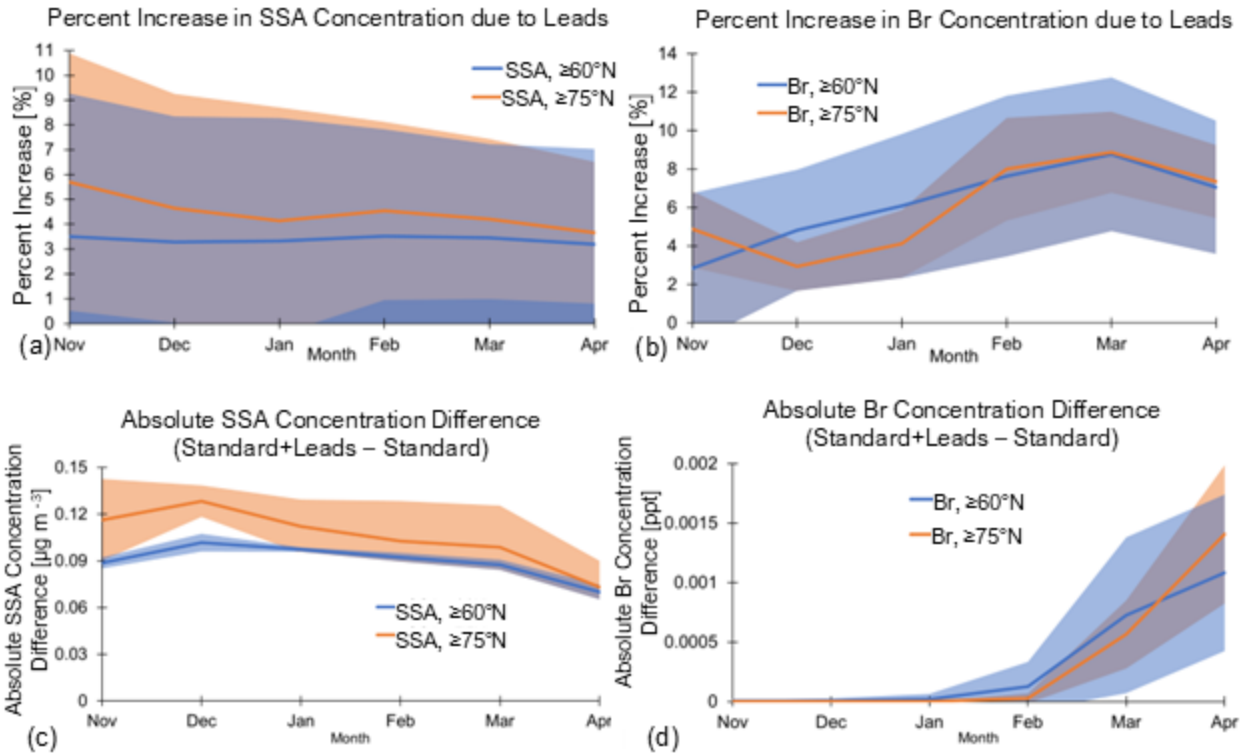
Figure 5. Multi-year (2002-2008) monthly mean percent increase due leads (calculated with Eq. (1)) in surface (a) SSA and (b) Br concentrations averaged across different Arctic regions (blue line: ≥60˚ N; orange line: ≥75˚ N). Shaded area represents ±1 standard deviation.

As described in Sect. 1, SSA contribute to the production of tropospheric reactive bromine and thereby bromine atom (Br). Here we examine changes in Br due to its role in ozone depletion events.
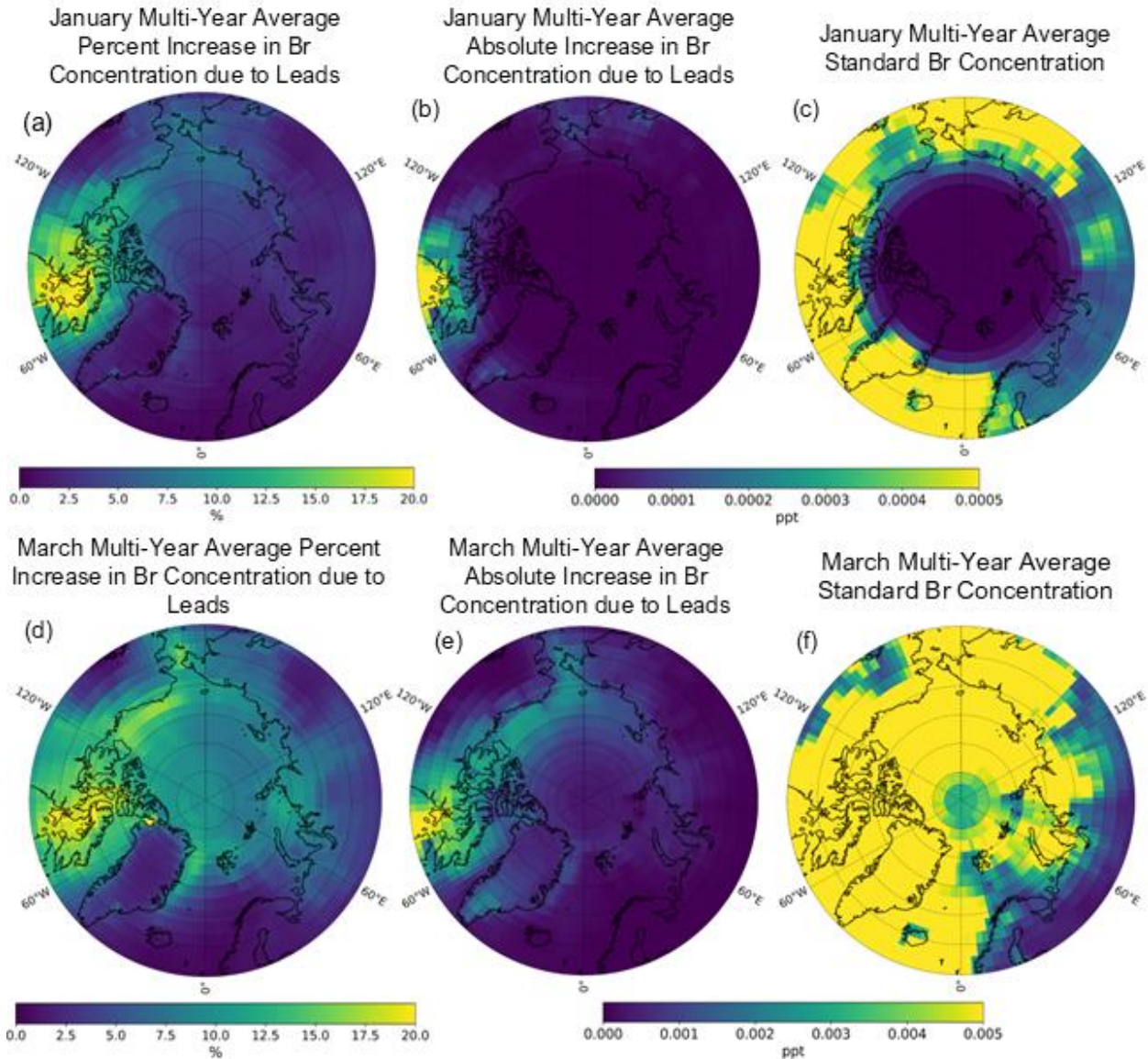
Figure 6- Multi-year (2002-2008) mean January (a, b, and c) and March (d, e, and f) percent increase due to leads in surface Br concentration (a and d), absolute increase in surface Br concentration due to leads (b and e), and the standard model surface Br concentration in ppt (c and f). Note the scale of the absolute difference and standard Br concentrations for the January and March multi-year averages are an order of magnitude difference.

Figure 6 shows the multi-year (2002-2008) mean percent increase and absolute difference due to leads in surface Br concentrations, and the standard Br concentration (in parts per trillion, or ppt) for the months of January (a-c) and March (d-f), respectively. Increased SSA from leads increases surface levels of Br across all months during the cold season (Fig. 6a, b, d, and e; Figs. S.6 and S.7 in the SI for other months). These increased concentrations spatially follow the

380   increased SSA mass concentrations from leads (Fig. 4a; Figs. S.4 and S.5 in SI for other months)

381   with differences due to where Br can be produced photochemically from the precursors released

382   from SSA. The spatial distribution of the percent increases in Br due to leads remains relatively

383   similar month to month during the cold season (see Fig. S.6 in SI), but with varying magnitude

384   (Fig. 6). The changes in Br concentration in February to April occur over a larger area (Fig. 6d

385   and e and Figs. S.6 and S.7), likely due to the seasonality of Arctic bromine chemistry, which is

386   influenced by increasing area where sunlight is available to photolyze Br-sourced SSA species.

387   The average Arctic-wide (≥60°N) percent increase due to leads in multi-year January mean

388   surface Br concentration is 6.1% and the maximum increase in an individual gridbox is 35%; for

389   March, it is 8.8% and 20.4%, respectively. Overall, the average monthly percent increase in Br

390   concentration is higher than the corresponding increases in SSA concentration, particularly after

391   January, and reaches a maximum in March (see Fig. 5). The percent change due to leads in Br

392   concentrations increases from November-March poleward of 60°N and from December-March

393   poleward of 75°N (Fig. 5b). This does not strictly follow the seasonality of lead emissions (Fig. 3)

394   or the percent increase in SSA concentrations due to leads (Fig. 5a), likely due to more available

395   sunlight for photochemical reactions that produce Br later in the cold season. Increases in surface

396   Br concentration could lead to decreased surface ozone concentrations. We find that the percent

397   decrease due to leads in average surface ozone concentrations during the Arctic cold season,

398   however, are negligible (< -0.25%).

399

400   *3.3 Evaluation Against Sea Salt Aerosol Observations*

401

402   We compare modeled and observed sodium (Na^+) mass concentrations at four long-term

403   monitoring stations to evaluate the performance of the simulation with and without additional lead

404   emissions. The locations of each observational site are shown in Fig. 4a.

405

406
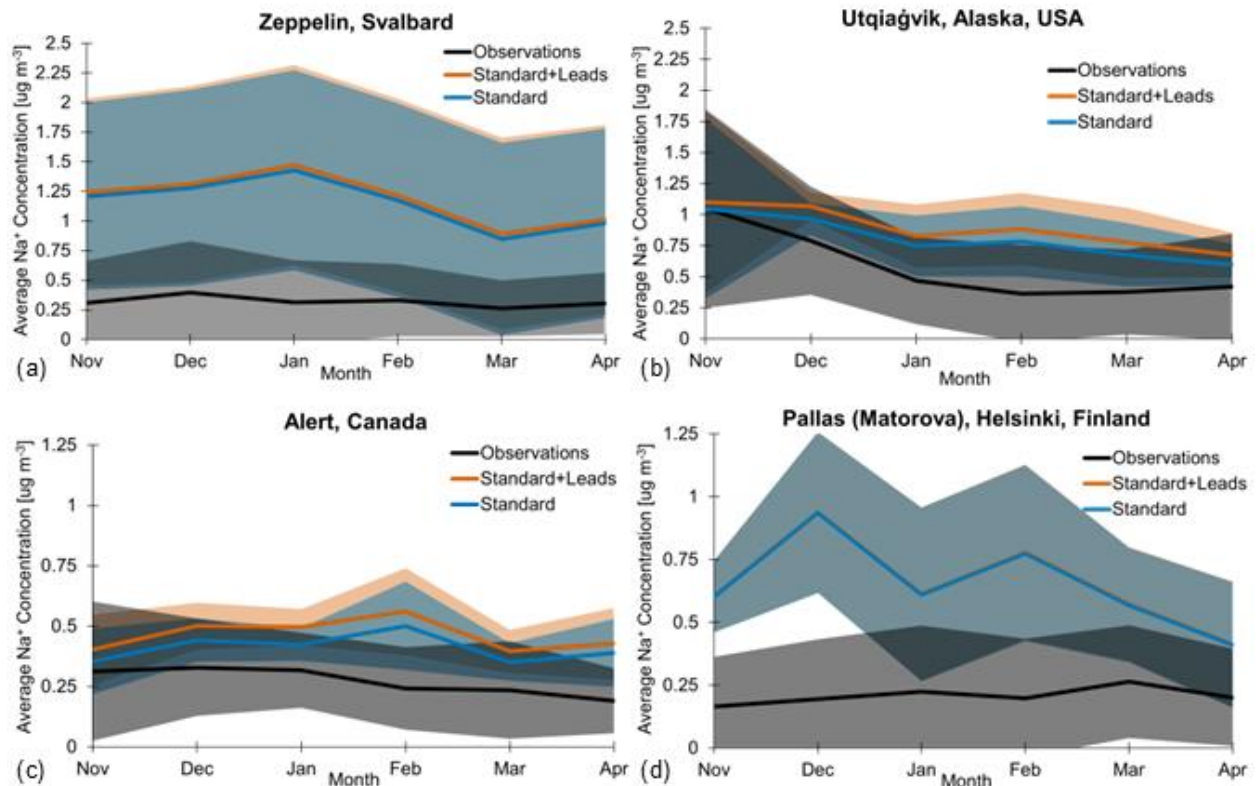
Figure 7- Observed (blackline) and simulated (blue and orange lines) multi-year monthly mean sodium mass concentrations at (a) Zeppelin, Norway, (b) Utqiaġvik, Alaska, (c) Alert, Canada, and (d) Pallas (Matorova), Helsinki, Finland for the cold seasons of 2002-2008 for (a)-(c) and 2003-2008 for (d). Shaded regions are ±1 standard deviation. Note the y-axis for Alert (c) and Pallas (d) are half as large as Zeppelin (a) and Utqiaġvik (b).

Figure 7 shows multi-year monthly mean Na$^+$ concentrations in the observations (black), standard + leads simulation (orange), and standard simulation (blue) for Zeppelin (a), Utqiaġvik (b), Alert (c), and Pallas (d) during the cold season for 2002-2008 (a-c) and 2003-2008 (d). We sample the model simulations in the gridbox that encompasses the latitude, longitude, and altitude of each monitoring station (see Sect. 2.3) and convert the simulated SSA to Na$^+$ concentrations. For all sites and months during the cold season, the simulated and observed Na$^+$ mass concentrations overlap within ± 1 standard deviation (shaded regions in Fig. 7), except in November and December at Pallas. We find mean concentrations are overpredicted in both the standard and standard + leads simulations at all sites and months during the cold season, apart from the standard model at Utqiaġvik and Alert in November which agree closest with observations.

425 The model overpredicts Na$^+$ concentrations the most at Zeppelin and Pallas, with the standard +

426 leads and standard mean concentrations a factor of 3.2 to 4.71 and 2.0 to 4.8 higher, respectively,

427 than observations across all months during the cold season. Confer et al. (2023) similarly find an

428 overprediction of SSA at Zeppelin, which they find is exacerbated by including blowing snow

429 emissions. Additionally, Zeppelin is at high elevation (located on a mountain at 475m) and has

430 been found to be more impacted by the free troposphere and aerosol-cloud interactions than other

431 Arctic sites (Freud et al., 2017); the chemical transport model cannot represent two-way aerosol-

432 cloud interactions. The model overestimate is less at Utqiaġvik, where the standard + leads

433 simulation still overpredicts observed concentrations by a factor of 1.0 to 2.4, and least at Alert,

434 with observed concentrations overestimated by a factor of 1.3 to 2.3 for the standard + leads

435 model. Lead emissions do not change the simulated seasonality of cold season surface SSA

436 concentrations. The timing of cold season maximum and minimum concentrations at Zeppelin,

437 Alert, and Pallas differs between the observed and simulated, for both the standard + leads and

438 standard models. At Utqiaġvik, the maximum mass concentration in the observations and both

439 model simulations occurs in November. However, the minimum observed cold season mass

440 concentration occurs in February at Utqiaġvik, whereas the standard + leads and standard mean

441 concentrations reach a minimum in April.

442

443 Figure 4a and b places the differences seen at each of the three sites in Fig. 7 into broader

444 context, with maps of the relative and absolute increases in SSA mass concentrations for the

445 month of January. There is minimal change in SSA concentrations where Pallas is located,

446 explaining the near equal Na$^+$ concentrations for the standard + leads and standard simulations

447 which results in the overlapping lines in Fig. 7d, suggesting minimal influence from leads at this

448 site. The most significant relative increase in SSA concentration from leads out of the four sites

449 occurs at Alert (Fig. 7a). However, regions with the largest changes in SSA mass concentration

450 due to leads in Fig. 4a and b for the month of January (i.e., parts of Northern Canada southwest

451 of Alert), which are consistent throughout the cold season (Fig. S.4 and S.5 in SI), are not sampled

452 by long-term ground monitoring sites, which would help constrain lead impacts on SSA. In our

453 simulation, lead emissions have the same size distribution as the open ocean, with most of the

454 mass in the coarse mode (82-90%). Despite this, there are increases in SSA concentration over

455 land (Fig. 4a and b) indicating transport (see also Text S.2 and Fig. S.8). This is consistent with

456 observed inland transport of SSA across the North Slope of Alaska (Simpson et al., 2005). It is

457 likely that leads emit smaller SSA particles relative to open ocean emissions (Nilsson et al., 2001),

458 which would increase their lifetime, so non-local impacts from leads may be greater than

459 simulated here. This further highlights the need for observations in other regions to better
460 understand the impacts of lead emissions.

461

462 There is strong observational evidence that lead emissions contribute to cold season SSA (see
463 Sect. 1), but the standard model consistently overpredicts observed SSA concentrations prior to
464 inclusion of additional lead emissions. This suggests other sources of SSA may be overpredicted
465 or sinks of SSA may be underpredicted. Ongoing work to improve the treatment of aerosol wet
466 removal processes in GEOS-Chem has not specifically investigated the impacts on sea salt
467 aerosol (Luo et al., 2020; Luo and Yu, 2023). Additionally, a recent observational study (Chen et
468 al., 2022) suggests that the GEOS-Chem blowing snow emissions parameterization may
469 overpredict the frequency of blowing snow events, therefore possibly contributing to the
470 overprediction of Arctic SSA mass concentrations.

471
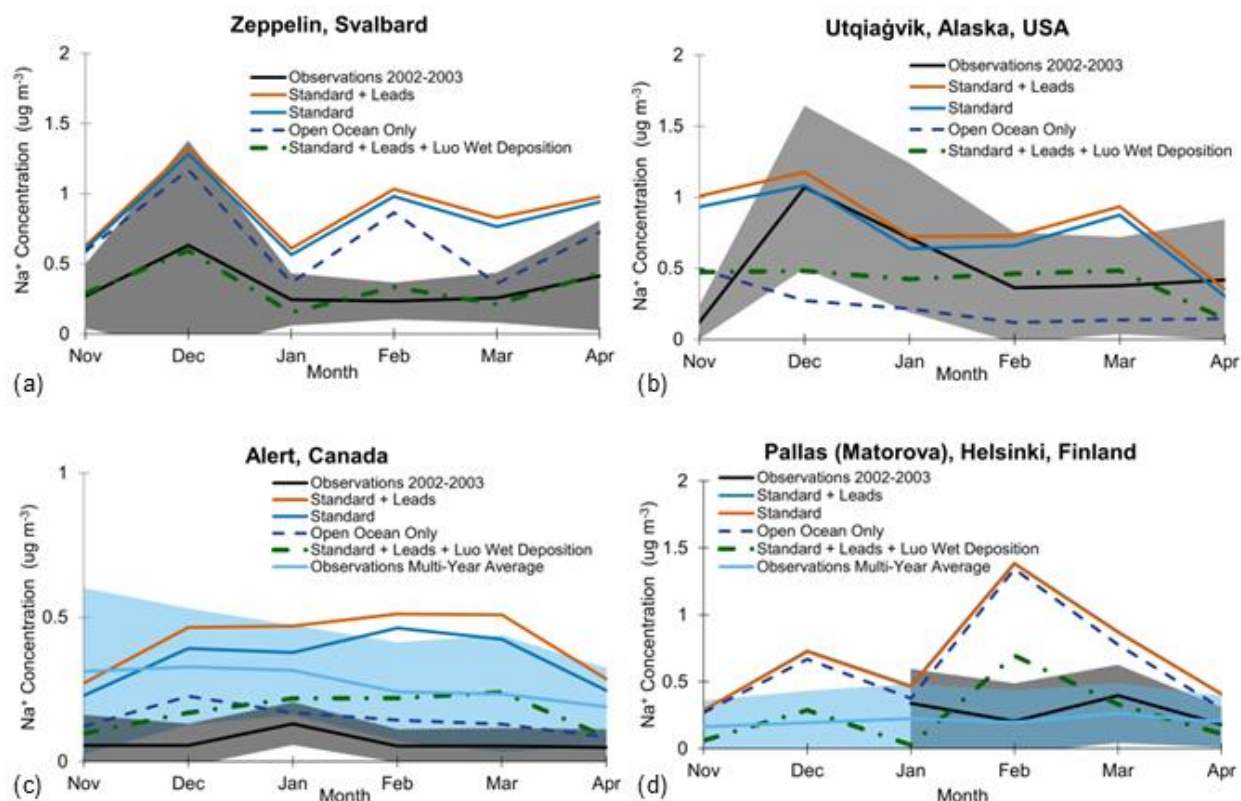
472

473 **Figure 8**- Model evaluation for the cold season 2002-2003 at Zeppelin (a), Utqiaġvik (b), Alert (c),
474 and Pallas (d). Observed Na+ concentrations are included as monthly averages for 2002-2003
475 (black + standard deviation margin), and the multi-year monthly averages (light blue + standard
476 deviation margin) (note: no 2002 data is available at Pallas). We show monthly average modeled
477 Na+ concentrations for 2002-2003 for the standard + leads (orange) and standard (blue)

478   simulations with two additional sensitivity studies: open ocean only emissions contributing to Na+

479   concentrations (dark blue with dashes) and the standard + leads emissions with Luo et al. (2020)

480   wet deposition applied (green line with dashes + dots). Note the different y-axis for Alert (c), as

481   concentrations are much lower at this site.

482

483   To test these possible sources of uncertainty, we run two additional sensitivity simulations for one

484   cold season (November 2002-April 2003): (1) using the Luo et al. (2020) wet deposition scheme

485   with the standard + leads SSA emissions ("standard + leads + Luo Wet Deposition") and (2)

486   turning off blowing snow emissions in the standard model for an "open ocean only" case (see Text

487   S.4 for further description). We find that the Luo wet deposition scheme improves model

488   agreement most at Zeppelin (see Fig. 8a), especially in the months of November, December,

489   March, and April. At Utqiaġvik, the Luo wet deposition scheme results in underestimates in Na$^+$

490   concentrations compared to observations (Fig. 8b) in December, January, and April and

491   overestimates in November, February, and March; however, the overestimated months are closer

492   to the observed concentrations than the standard + leads and standard simulations. Additionally,

493   the standard model at Utqiaġvik agrees with observations in December and the standard + leads

494   model agrees with observations in January and April.

495

496   At Alert, the Luo wet deposition scheme decreases the model overestimate of the standard +

497   leads simulation when compared to the observations for the 2002-2003 cold season (Fig. 8c), but

498   still overestimates Na$^+$ concentrations in each month. As the 2002-2003 observations at Alert are

499   particularly low, we also include the observed multi-year (2002-2008) monthly average Na$^+$

500   concentrations for comparison. The Luo wet deposition scheme improves model evaluation from

501   February-March compared to the multi-year average observed concentrations at Alert, but

502   otherwise underpredicts concentrations. The Luo wet deposition scheme decreases

503   overprediction at Pallas in February compared to observations from the 2003 cold season and

504   improves model agreement in March and April, but underpredicts Na$^+$ concentrations in January

505   (Fig. 8d). As there are no available observations in 2002 at Pallas, we also include the observed

506   multi-year (2003-2008) monthly average Na$^+$ concentrations for comparison. The Luo wet

507   deposition scheme underpredicts Na$^+$ concentrations in November, January, and April and

508   overpredicts concentrations in December and March compared to the multi-year average

509   concentrations at Pallas.

510

At Utqiaġvik, under predicted Na$^+$ concentrations with only open ocean emissions (except in November) suggest that this site is influenced by blowing snow emissions and/or lead emissions. Of the four sites, blowing snow is most important and well-represented here, as it also improves the modeled seasonality by correctly representing the December peak in Na$^+$ concentrations in the standard + leads and standard model; there may be larger uncertainty in the emissions parameterization in other regions. At Zeppelin, Alert, and Pallas, even with open ocean emissions only and the standard wet deposition, the model overestimates Na$^+$ concentrations for all months during the cold season for 2002-2003, except at Pallas in January, where only open ocean emissions more closely match observations. Moreover, the open ocean only Na$^+$ concentrations are close in value to the standard + leads and standard concentrations, indicating Pallas is largely influenced by open ocean emissions, rather than blowing snow and lead emissions.

The results of these sensitivity tests suggest that changes to wet scavenging may be more important at higher altitudes, given the improvement in model evaluation at Zeppelin. Yet, the inclusion of the Luo wet deposition scheme to the standard+leads simulation still overestimates concentrations at Alert, and generally leads to disagreement with observations at Utqiaġvik and Pallas (except in March and April at Pallas).

4. Uncertainties Discussion

Our model evaluation reveals SSA is overestimated in the standard and standard + leads model at each of the 4 Arctic sampling sites, pointing to possible sources of uncertainty. First, we use the Jaeglé et al. (2011) open ocean function for our lead emissions parameterization as it is the standard SSA emission function in GEOS-Chem that has been previously evaluated across global oceans. However, there are possible differences in the mechanisms and meteorological dependencies of SSA emission from leads vs. the open ocean which could impact the magnitude and spatial patterns of lead emissions. Some potential differences were investigated in a summertime measurement study (Nilsson et al., 2001), where they derive an empirical lead emissions flux equation with an exponential dependence on windspeed and no consideration of SST (Eq. (S.2) in SI). They found the emissions rate per area from leads is smaller than that of the open ocean due to lower fetch in leads, which suggests the lead emissions estimated in our study may be an upper limit when considering large leads only (>3km in size); however, this lead fraction detected by AMSR-E may only include 50% of total lead area (Röhrs and Kaleschke, 2012). Additionally, Nilsson et al. (2001) suggest leads emit smaller SSA particles relative to the

545   open ocean, which would increase their lifetime and transport distance. To create a more robust
546   understanding of the different SSA emission mechanisms from leads vs. the open ocean, more
547   studies using size-resolved observations could be conducted within the areas we predict the
548   highest lead emissions, such as within the Bering Strait, Nares Strait, Wynniatt Bay in the
549   Canadian archipelago, and the eastern Greenland Sea.

550

551   Our sensitivity study results do not ultimately confirm the source(s) of overprediction within the
552   GEOS-Chem model. Blowing snow emissions are included as a standard source of SSA
553   emissions in the Arctic, but remaining uncertainties about the GEOS-Chem blowing snow
554   emissions parameterization (Chen et al., 2022) suggest a need for refinement. Additionally, the
555   results of the standard + leads + Luo wet deposition simulation highlight there are remaining
556   uncertainties associated with wet deposition schemes as the Luo et al. (2020) mechanism does
557   not lead to consistent improvement of simulated SSA concentrations. Luo & Yu (2023) find that
558   the scheme overestimates wet scavenging on a global scale, so continued improvement in the
559   model deposition processes may resolve SSA overestimates.

560

561   5. **Conclusions**

562

563   Observational evidence (Chen et al., 2022; Kirpes et al., 2019; May et al., 2016; Radke et al.,
564   1976; Scott and Levin, 1972; Willis et al., 2018) and one modeling study of the 400 km^2 region
565   around Utqiaġvik, Alaska (Ioannidis et al., 2023) have shown that leads may be an important
566   source of cold season SSA for the coastal Arctic. Here, we evaluate their importance as an Arctic-
567   wide source of cold season SSA emissions and their potential atmospheric chemistry impacts in
568   the global chemical transport model GEOS-Chem.

569

570   We find that lead SSA emissions occur primarily in regions where other SSA emissions sources
571   are very low, mainly within the Bering Strait, Nares Strait, Wynniatt Bay in the Canadian
572   archipelago, and the eastern Greenland Sea. Poleward of 75˚ N, leads increase total monthly
573   cold-season SSA emissions by 5.6 to 7.5%, with the highest contribution of SSA emissions from
574   leads in January and the lowest in April. Lead emissions vary in magnitude by month and year,
575   mainly due to variations in lead area. Future trends in Arctic sea ice predicted by climate models
576   suggest a possible future increasing trend in lead area (Intergovernmental Panel On Climate
577   Change, 2023), which would increase lead emissions. The additional SSA from leads in regions
578   where the background aerosol concentrations are low could also affect local aerosol-cloud

interactions, but the overall warming or cooling effect of these additional aerosols remains uncertain (Cox et al., 2015; Schmale et al., 2021; Stramler et al., 2011; Tan et al., 2023; Villanueva et al., 2022).

SSA mass concentrations increase primarily at the location of lead emissions, in regions where the standard SSA mass concentration is very low (≤1.2 µg m^{-3}). Throughout the cold season, the increased SSA mass concentrations from leads remain relatively constant in magnitude and spatial distribution. The highest increase in multi-year average SSA mass concentrations due to leads, spatially averaged for ≥75°N, occurs in November (5.7% ± 5.2%) and the lowest occurs in April (3.7% ± 2.9%). Increased SSA from leads increases surface Br concentrations during the cold season in corresponding locations. We find total Arctic-wide (≥60°N) increases in multi-year mean surface Br concentration range from 2.8 to 8.8%. The increases in Br are not sufficient to have an impact on ozone; subsequent decreases in average surface ozone concentrations in the Arctic are negligible (< -0.25%).

Overall, we predict sea ice leads may impact Arctic-wide cold-season SSA concentrations and Br concentrations by up to 5-10% on average during the 2002-2008 period. As leads are likely to increase in prevalence under climate change, including this source of SSA in chemistry and climate models may become more important for future predictions.

Code and Data Availability

Standard model code: https://doi.org/10.5281/zenodo.5500717; AMSR-E data: https://www.cen.uni-hamburg.de/en/icdc/data/cryosphere/lead-area-fraction-amsre.html); observational site data (Alert, Pallas, and Zeppelin): https://ebas-data.nilu.no/Default.aspx; observational data (Utqiaġvik): https://saga.pmel.noaa.gov/data/stations/; model data shown in paper: https://doi.org/10.5281/zenodo.14611355.

Author Contribution

EJE was responsible for data curation, model simulations, validation, visualization, and analysis with expert advice from HMH. HMH is responsible for conceptualization. EJE drafted the manuscript which was revised by HMH.

Competing Interests

The authors declare that they have no conflict of interest.

Acknowledgements

We thank Kerri Pratt for helpful discussions. HMH was supported by Department of Energy (DOE) Atmospheric Systems Research (ASR), award DE-SC0023049. We acknowledge financial support from the department of Civil and Environmental Engineering at the University of Illinois Urbana-Champaign.

Supplemental Information

Equations of SSA flux from Jaegle et a. (2011) and Nilsson et al. (2001); Additional figures of lead SSA emissions for months other than January during the cold season; Cold season total lead SSA emissions; Description and figure of the correlation between lead area and lead SSA emissions; long-term trends in lead area (2002-2011) and relevant statistical testing; additional figures of multi-year (2002-2008) mean percent increase due to leads in SSA and bromine concentration for months other than January during the cold season; Description and figures of correlation between lead emissions and coarse and accumulation mode SSA concentration; Sensitivity simulations.

6. **References**

Abbatt, J. P. D., Thomas, J. L., Abrahamsson, K., Boxe, C., Granfors, A., Jones, A. E., King, M. D., Saiz-Lopez, A., Shepson, P. B., Sodeau, J., Toohey, D. W., Toubin, C., Von Glasow, R., Wren, S. N., and Yang, X.: Halogen activation via interactions with environmental ice and snow in the polar lower troposphere and other regions, Atmospheric Chem. Phys., 12, 6237–6271, https://doi.org/10.5194/acp-12-6237-2012, 2012.

Alvarez-Aviles, L., Simpson, W. R., Douglas, T. A., Sturm, M., Perovich, D., and Domine, F.: Frost flower chemical composition during growth and its implications for aerosol production and bromine activation, J. Geophys. Res. Atmospheres, 113, 2008JD010277, https://doi.org/10.1029/2008JD010277, 2008.

Amos, H. M., Jacob, D. J., Holmes, C. D., Fisher, J. A., Wang, Q., Yantosca, R. M., Corbitt, E. S., Galarneau, E., Rutter, A. P., Gustin, M. S., Steffen, A., Schauer, J. J., Graydon, J. A., Louis, V. L. St., Talbot, R. W., Edgerton, E. S., Zhang, Y., and Sunderland, E. M.: Gas-particle partitioning of atmospheric Hg(II) and its effect on global mercury deposition, Atmospheric Chem. Phys., 12, 591–603, https://doi.org/10.5194/acp-12-591-2012, 2012.

Chen, Q., Mirrielees, J. A., Thanekar, S., Loeb, N. A., Kirpes, R. M., Upchurch, L. M., Barget, A. J., Lata, N. N., Raso, A. R. W., McNamara, S. M., China, S., Quinn, P. K., Ault, A. P., Kennedy, A., Shepson, P. B., Fuentes, J. D., and Pratt, K. A.: Atmospheric particle abundance and sea salt aerosol observations in the springtime Arctic: a focus on blowing snow and leads, Atmospheric Chem. Phys., 22, 15263–15285, https://doi.org/10.5194/acp-22-15263-2022, 2022.

649   Confer, K. L., Jaeglé, L., Liston, G. E., Sharma, S., Nandan, V., Yackel, J., Ewert, M., and Horowitz, H. M.:
650   Impact of Changing Arctic Sea Ice Extent, Sea Ice Age, and Snow Depth on Sea Salt Aerosol From Blowing
651   Snow and the Open Ocean for 1980–2017, J. Geophys. Res. Atmospheres, 128, e2022JD037667,
652   https://doi.org/10.1029/2022JD037667, 2023.

653   Cox, C. J., Walden, V. P., Rowe, P. M., and Shupe, M. D.: Humidity trends imply increased sensitivity to
654   clouds in a warming Arctic, Nat. Commun., 6, 10117, https://doi.org/10.1038/ncomms10117, 2015.

655   DeMott, P. J., Hill, T. C. J., McCluskey, C. S., Prather, K. A., Collins, D. B., Sullivan, R. C., Ruppel, M. J.,
656   Mason, R. H., Irish, V. E., Lee, T., Hwang, C. Y., Rhee, T. S., Snider, J. R., McMeeking, G. R., Dhaniyala, S.,
657   Lewis, E. R., Wentzell, J. J. B., Abbatt, J., Lee, C., Sultana, C. M., Ault, A. P., Axson, J. L., Diaz Martinez, M.,
658   Venero, I., Santos-Figueroa, G., Stokes, M. D., Deane, G. B., Mayol-Bracero, O. L., Grassian, V. H., Bertram,
659   T. H., Bertram, A. K., Moffett, B. F., and Franc, G. D.: Sea spray aerosol as a unique source of ice
660   nucleating particles, Proc. Natl. Acad. Sci., 113, 5797–5803, https://doi.org/10.1073/pnas.1514034112,
661   2016.

662   Dibb, J. E., Ziemba, L. D., Luxford, J., and Beckman, P.: Bromide and other ions in the snow, firn air, and
663   atmospheric boundary layer at Summit during GSHOX, Atmospheric Chem. Phys., 10, 9931–9942,
664   https://doi.org/10.5194/acp-10-9931-2010, 2010.

665   Domine, F., Sparapani, R., Ianniello, A., and Beine, H. J.: The origin of sea salt in snow on Arctic sea ice
666   and in coastal regions, Atmospheric Chem. Phys., 4, 2259–2271, https://doi.org/10.5194/acp-4-2259-
667   2004, 2004.

668   Freud, E., Krejci, R., Tunved, P., Leaitch, R., Nguyen, Q. T., Massling, A., Skov, H., and Barrie, L.: Pan-Arctic
669   aerosol number size distributions: seasonality and transport patterns, Atmospheric Chem. Phys., 17,
670   8101–8128, https://doi.org/10.5194/acp-17-8101-2017, 2017.

671   Gelaro, R., McCarty, W., Suárez, M. J., Todling, R., Molod, A., Takacs, L., Randles, C. A., Darmenov, A.,
672   Bosilovich, M. G., Reichle, R., Wargan, K., Coy, L., Cullather, R., Draper, C., Akella, S., Buchard, V., Conaty,
673   A., Da Silva, A. M., Gu, W., Kim, G.-K., Koster, R., Lucchesi, R., Merkova, D., Nielsen, J. E., Partyka, G.,
674   Pawson, S., Putman, W., Rienecker, M., Schubert, S. D., Sienkiewicz, M., and Zhao, B.: The Modern-Era
675   Retrospective Analysis for Research and Applications, Version 2 (MERRA-2), J. Clim., 30, 5419–5454,
676   https://doi.org/10.1175/JCLI-D-16-0758.1, 2017.

677   Gong, S. L.: A parameterization of sea-salt aerosol source function for sub- and super-micron particles,
678   Glob. Biogeochem. Cycles, 17, 2003GB002079, https://doi.org/10.1029/2003GB002079, 2003.

679   Huang, J. and Jaeglé, L.: Wintertime enhancements of sea salt aerosol in polar regions consistent with a
680   sea ice source from blowing snow, Atmospheric Chem. Phys., 17, 3699–3712,
681   https://doi.org/10.5194/acp-17-3699-2017, 2017.

682   Huang, J., Jaeglé, L., and Shah, V.: Using CALIOP to constrain blowing snow emissions of sea salt aerosols
683   over Arctic and Antarctic sea ice, Atmospheric Chem. Phys., 18, 16253–16269,
684   https://doi.org/10.5194/acp-18-16253-2018, 2018.

685   Huang, J., Jaeglé, L., Chen, Q., Alexander, B., Sherwen, T., Evans, M. J., Theys, N., and Choi, S.: Evaluating
686   the impact of blowing-snow sea salt aerosol on springtime BrO and O_3 in the
687   Arctic, Atmospheric Chem. Phys., 20, 7335–7358, https://doi.org/10.5194/acp-20-7335-2020, 2020.

688   Integrated Climate Data Center (ICDC), CEN, and University of Hamburg, Hamburg, Germany: AMSR-E
689   Arctic lead area fraction, n.d.

690   Intergovernmental Panel On Climate Change: Climate Change 2021 – The Physical Science Basis: Working
691   Group I Contribution to the Sixth Assessment Report of the Intergovernmental Panel on Climate Change,
692   1st ed., Cambridge University Press, https://doi.org/10.1017/9781009157896, 2023.

693   Ioannidis, E., Law, K. S., Raut, J.-C., Marelle, L., Onishi, T., Kirpes, R. M., Upchurch, L. M., Tuch, T.,
694   Wiedensohler, A., Massling, A., Skov, H., Quinn, P. K., and Pratt, K. A.: Modelling wintertime sea-spray
695   aerosols under Arctic haze conditions, Atmospheric Chem. Phys., 23, 5641–5678,
696   https://doi.org/10.5194/acp-23-5641-2023, 2023.

697   Jaeglé, L., Quinn, P. K., Bates, T. S., Alexander, B., and Lin, J.-T.: Global distribution of sea salt aerosols:
698   new constraints from in situ and remote sensing observations, Atmospheric Chem. Phys., 11, 3137–3157,
699   https://doi.org/10.5194/acp-11-3137-2011, 2011.

700   Keller, C. A., Long, M. S., Yantosca, R. M., Da Silva, A. M., Pawson, S., and Jacob, D. J.: HEMCO v1.0: a
701   versatile, ESMF-compliant component for calculating emissions in atmospheric models, Geosci. Model
702   Dev., 7, 1409–1417, https://doi.org/10.5194/gmd-7-1409-2014, 2014.

703   Kirpes, R. M., Bonanno, D., May, N. W., Fraund, M., Barget, A. J., Moffet, R. C., Ault, A. P., and Pratt, K. A.:
704   Wintertime Arctic Sea Spray Aerosol Composition Controlled by Sea Ice Lead Microbiology, ACS Cent.
705   Sci., 5, 1760–1767, https://doi.org/10.1021/acscentsci.9b00541, 2019.

706   Leaitch, W. R., Russell, L. M., Liu, J., Kolonjari, F., Toom, D., Huang, L., Sharma, S., Chivulescu, A., Veber,
707   D., and Zhang, W.: Organic functional groups in the submicron aerosol at 82.5° N, 62.5° W from 2012 to
708   2014, Atmospheric Chem. Phys., 18, 3269–3287, https://doi.org/10.5194/acp-18-3269-2018, 2018.

709   Lin, H., Jacob, D. J., Lundgren, E. W., Sulprizio, M. P., Keller, C. A., Fritz, T. M., Eastham, S. D., Emmons, L.
710   K., Campbell, P. C., Baker, B., Saylor, R. D., and Montuoro, R.: Harmonized Emissions Component
711   (HEMCO) 3.0 as a versatile emissions component for atmospheric models: application in the GEOS-
712   Chem, NASA GEOS, WRF-GC, CESM2, NOAA GEFS-Aerosol, and NOAA UFS models, Geosci. Model Dev.,
713   14, 5487–5506, https://doi.org/10.5194/gmd-14-5487-2021, 2021.

714   Liu, H., Jacob, D. J., Bey, I., and Yantosca, R. M.: Constraints from ^{210}Pb and [7]Be on wet deposition and
715   transport in a global three-dimensional chemical tracer model driven by assimilated meteorological
716   fields, J. Geophys. Res. Atmospheres, 106, 12109–12128, https://doi.org/10.1029/2000JD900839, 2001.

717   Luo, G. and Yu, F.: Impact of Air Refreshing and Cloud Ice Uptake Limitations on Vertical Profiles and Wet
718   Depositions of Nitrate, Ammonium, and Sulfate, Geophys. Res. Lett., 50, e2023GL104258,
719   https://doi.org/10.1029/2023GL104258, 2023.

720   Luo, G., Yu, F., and Moch, J. M.: Further improvement of wet process treatments in GEOS-Chem v12.6.0:
721   impact on global distributions of aerosols and aerosol precursors, Geosci. Model Dev., 13, 2879–2903,
722   https://doi.org/10.5194/gmd-13-2879-2020, 2020.

723   May, N. W., Quinn, P. K., McNamara, S. M., and Pratt, K. A.: Multiyear study of the dependence of sea salt
724   aerosol on wind speed and sea ice conditions in the coastal Arctic, J. Geophys. Res. Atmospheres, 121,
725   9208–9219, https://doi.org/10.1002/2016JD025273, 2016.

726 Monahan, E. C., Spiel, D. E., and Davidson, K. L.: A Model of Marine Aerosol Generation Via Whitecaps
727 and Wave Disruption, in: Oceanic Whitecaps, vol. 2, edited by: Monahan, E. C. and Niocaill, G. M.,
728 Springer Netherlands, Dordrecht, 167–174, https://doi.org/10.1007/978-94-009-4668-2_16, 1986.

729 Nilsson, E. D., Rannik, Ü., Swietlicki, E., Leck, C., Aalto, P. P., Zhou, J., and Norman, M.: Turbulent aerosol
730 fluxes over the Arctic Ocean: 2. Wind-driven sources from the sea, J. Geophys. Res. Atmospheres, 106,
731 32139–32154, https://doi.org/10.1029/2000JD900747, 2001.

732 Pierce, J. R. and Adams, P. J.: Global evaluation of CCN formation by direct emission of sea salt and
733 growth of ultrafine sea salt, J. Geophys. Res. Atmospheres, 111, 2005JD006186,
734 https://doi.org/10.1029/2005JD006186, 2006.

735 Pound, R. J., Sherwen, T., Helmig, D., Carpenter, L. J., and Evans, M. J.: Influences of oceanic ozone
736 deposition on tropospheric photochemistry, Atmospheric Chem. Phys., 20, 4227–4239,
737 https://doi.org/10.5194/acp-20-4227-2020, 2020.

738 Pratt, K. A., Custard, K. D., Shepson, P. B., Douglas, T. A., Pöhler, D., General, S., Zielcke, J., Simpson, W. R.,
739 Platt, U., Tanner, D. J., Gregory Huey, L., Carlsen, M., and Stirm, B. H.: Photochemical production of
740 molecular bromine in Arctic surface snowpacks, Nat. Geosci., 6, 351–356,
741 https://doi.org/10.1038/ngeo1779, 2013.

742 Quinn, P. K., Coffman, D. J., Kapustin, V. N., Bates, T. S., and Covert, D. S.: Aerosol optical properties in the
743 marine boundary layer during the First Aerosol Characterization Experiment (ACE 1) and the underlying
744 chemical and physical aerosol properties, J. Geophys. Res., 103, 16,547-16,563, 1998.

745 Quinn, P. K., Bates, T. S., Miller, T. L., Coffman, D. J., Johnson, J. E., Harris, J. M., Ogren, J. A., Forbes, G.,
746 Anderson, T. L., Covert, D. S., and Rood, M. J.: Surface submicron aerosol chemical composition: What
747 fraction is not sulfate?, J. Geophys. Res. Atmospheres, 105, 6785–6805,
748 https://doi.org/10.1029/1999JD901034, 2000.

749 Quinn, P. K., Miller, T. L., Bates, T. S., Ogren, J. A., Andrews, E., and Shaw, G. E.: A 3-year record of
750 simultaneously measured aerosol chemical and optical properties at Barrow, Alaska, J. Geophys. Res.
751 Atmospheres, 107, https://doi.org/10.1029/2001JD001248, 2002.

752 Radke, L. F., Hobbs, P. V., and Pinnons, J. E.: Observations of Cloud Condensation Nuclei, Sodium-
753 Containing Particles, Ice Nuclei and the Light-Scattering Coefficient Near Barrow, Alaska, J. Appl. Meteor.
754 Climatol., 15, 982–995, https://doi.org/10.1175/1520-0450(1976)015%3C0982:OOCCNS%3E2.0.CO;2,
755 1976.

756 Rhodes, R. H., Yang, X., Wolff, E. W., McConnell, J. R., and Frey, M. M.: Sea ice as a source of sea salt
757 aerosol to Greenland ice cores: a model-based study, Atmospheric Chem. Phys., 17, 9417–9433,
758 https://doi.org/10.5194/acp-17-9417-2017, 2017.

759 Riley, J. P. and Chester, R.: Introduction to marine chemistry, Academic Press, London, New York, 465 pp.,
760 1971.

761 Röhrs, J. and Kaleschke, L.: An algorithm to detect sea ice leads by using AMSR-E passive microwave
762 imagery, The Cryosphere, 6, 343–352, https://doi.org/10.5194/tc-6-343-2012, 2012.

763 Roscoe, H. K., Brooks, B., Jackson, A. V., Smith, M. H., Walker, S. J., Obbard, R. W., and Wolff, E. W.: Frost
764 flowers in the laboratory: Growth, characteristics, aerosol, and the underlying sea ice, J. Geophys. Res.,
765 116, D12301, https://doi.org/10.1029/2010JD015144, 2011.

766 Salmi, T.: Measurement of Inorganics in air and particle phase at Pallas (Matorova) (3),
767 https://doi.org/10.48597/T6MX-CEKH, 2018.

768 Schmale, J., Zieger, P., and Ekman, A. M. L.: Aerosols in current and future Arctic climate, Nat. Clim.
769 Change, 11, 95–105, https://doi.org/10.1038/s41558-020-00969-5, 2021.

770 Scott, W. D. and Levin, Z.: Open Channels in Sea Ice (Leads) as Ion Sources, Science, 177, 425–426,
771 https://doi.org/10.1126/science.177.4047.425, 1972.

772 Screen, J. A. and Simmonds, I.: Declining summer snowfall in the Arctic: causes, impacts and feedbacks,
773 Clim. Dyn., 38, 2243–2256, https://doi.org/10.1007/s00382-011-1105-2, 2012.

774 Simpson, W. R., Alvarez-Aviles, L., Douglas, T. A., Sturm, M., and Domine, F.: Halogens in the coastal snow
775 pack near Barrow, Alaska: Evidence for active bromine air-snow chemistry during springtime, Geophys.
776 Res. Lett., 32, 2004GL021748, https://doi.org/10.1029/2004GL021748, 2005.

777 Simpson, W. R., Von Glasow, R., Riedel, K., Anderson, P., Ariya, P., Bottenheim, J., Burrows, J., Carpenter,
778 L. J., Frieß, U., Goodsite, M. E., Heard, D., Hutterli, M., Jacobi, H.-W., Kaleschke, L., Neff, B., Plane, J., Platt,
779 U., Richter, A., Roscoe, H., Sander, R., Shepson, P., Sodeau, J., Steffen, A., Wagner, T., and Wolff, E.:
780 Halogens and their role in polar boundary-layer ozone depletion, Atmospheric Chem. Phys., 7, 4375–
781 4418, https://doi.org/10.5194/acp-7-4375-2007, 2007.

782 Stramler, K., Del Genio, A. D., and Rossow, W. B.: Synoptically Driven Arctic Winter States, J. Clim., 24,
783 1747–1762, https://doi.org/10.1175/2010JCLI3817.1, 2011.

784 Stutz, J., Thomas, J. L., Hurlock, S. C., Schneider, M., Von Glasow, R., Piot, M., Gorham, K., Burkhart, J. F.,
785 Ziemba, L., Dibb, J. E., and Lefer, B. L.: Longpath DOAS observations of surface BrO at Summit, Greenland,
786 Atmospheric Chem. Phys., 11, 9899–9910, https://doi.org/10.5194/acp-11-9899-2011, 2011.

787 Sumata, H., De Steur, L., Divine, D. V., Granskog, M. A., and Gerland, S.: Regime shift in Arctic Ocean sea
788 ice thickness, Nature, 615, 443–449, https://doi.org/10.1038/s41586-022-05686-x, 2023.

789 Swanson, W. F., Holmes, C. D., Simpson, W. R., Confer, K., Marelle, L., Thomas, J. L., Jaeglé, L., Alexander,
790 B., Zhai, S., Chen, Q., Wang, X., and Sherwen, T.: Comparison of model and ground observations finds
791 snowpack and blowing snow aerosols both contribute to Arctic tropospheric reactive bromine,
792 Atmospheric Chem. Phys., 22, 14467–14488, https://doi.org/10.5194/acp-22-14467-2022, 2022.

793 Tan, I., Sotiropoulou, G., Taylor, P. C., Zamora, L., and Wendisch, M.: A Review of the Factors Influencing
794 Arctic Mixed-Phase Clouds: Progress and Outlook, in: Geophysical Monograph Series, edited by: Sullivan,
795 S. C. and Hoose, C., Wiley, 103–132, https://doi.org/10.1002/9781119700357.ch5, 2023.

796 Vaughan, D., Comiso, J., Allison, I., Carrasco, J., Kaser, G., Kwok, R., Mote, P., Murray, T., Paul, F., Ren, J. F.,
797 Rignot, E., Solomina, O., Steffen, K., and Zhang, T.: Observations: Cryosphere, in: Climate Change 2013:
798 The Physical Science Basis, 317–382, 2013.

799 Villanueva, D., Possner, A., Neubauer, D., Gasparini, B., Lohmann, U., and Tesche, M.: Mixed-phase
800 regime cloud thinning could help restore sea ice, Environ. Res. Lett., 17, 114057,
801 https://doi.org/10.1088/1748-9326/aca16d, 2022.

802 Wang, Q., Jacob, D. J., Spackman, J. R., Perring, A. E., Schwarz, J. P., Moteki, N., Marais, E. A., Ge, C.,
803 Wang, J., and Barrett, S. R. H.: Global budget and radiative forcing of black carbon aerosol: Constraints
804 from pole-to-pole (HIPPO) observations across the Pacific, J. Geophys. Res. Atmospheres, 119, 195–206,
805 https://doi.org/10.1002/2013JD020824, 2014.

806 Wang, X., Jacob, D. J., Downs, W., Zhai, S., Zhu, L., Shah, V., Holmes, C. D., Sherwen, T., Alexander, B.,
807 Evans, M. J., Eastham, S. D., Neuman, J. A., Veres, P. R., Koenig, T. K., Volkamer, R., Huey, L. G., Bannan, T.
808 J., Percival, C. J., Lee, B. H., and Thornton, J. A.: Global tropospheric halogen (Cl, Br, I) chemistry and its
809 impact on oxidants, Atmospheric Chem. Phys., 21, 13973–13996, https://doi.org/10.5194/acp-21-13973-
810 2021, 2021.

811 Wang, Y., Jacob, D. J., and Logan, J. A.: Global simulation of tropospheric O_3-NO_x-hydrocarbon
812 chemistry: 3. Origin of tropospheric ozone and effects of nonmethane hydrocarbons, J. Geophys. Res.
813 Atmospheres, 103, 10757–10767, https://doi.org/10.1029/98JD00156, 1998.

814 Willis, M. D., Leaitch, W. R., and Abbatt, J. P. D.: Processes Controlling the Composition and Abundance of
815 Arctic Aerosol, Rev. Geophys., 56, 621–671, https://doi.org/10.1029/2018RG000602, 2018.

816 World Meteorological Organization (WMO): WMO/GAW aerosol measurement procedures, guidelines
817 and recommendations, WMO, Geneva, 2003.

818 Yang, X., Neděla, V., Runštuk, J., Ondrušková, G., Krausko, J., Vetráková, Ľ., and Heger, D.: Evaporating
819 brine from frost flowers with electron microscopy and implications for atmospheric chemistry and sea-
820 salt aerosol formation, Atmospheric Chem. Phys., 17, 6291–6303, https://doi.org/10.5194/acp-17-6291-
821 2017, 2017.

822 Zhang, L., Gong, S., Padro, J., and Barrie, L.: A size-segregated particle dry deposition scheme for an
823 atmospheric aerosol module, Atmos. Environ., 35, 549–560, 2001.

824